

Visualizing crystal twin boundaries of bismuth by high-spatial-resolution ARPES

Ayumi Moriya ¹, Kosuke Nakayama ^{1,2,*}, Tappei Kawakami ¹, Kensaku Maeda ³, Atsuya Tokuyama,¹ Seigo Souma ^{4,5},
Chaoyu Chen ^{6,†}, José Avila ⁶, Maria Carmen Asensio,⁷ Miho Kitamura,⁸ Koji Horiba,⁹ Hiroshi Kumigashira ¹⁰,
Takashi Takahashi,¹ Kozo Fujiwara ³, Kouji Segawa ¹¹ and Takafumi Sato^{1,4,5,12,‡}

¹Department of Physics, Graduate School of Science, Tohoku University, Sendai 980-8578, Japan

²Precursory Research for Embryonic Science and Technology (PRESTO), Japan Science and Technology Agency (JST),
Tokyo 102-0076, Japan

³Institute for Materials Research, Tohoku University, Sendai 980-8577, Japan

⁴Advanced Institute for Materials Research, Tohoku University, Sendai 980-8577, Japan

⁵Center for Science and Innovation in Spintronics (CSIS), Tohoku University, Sendai 980-8577, Japan

⁶Synchrotron SOLEIL, L'Orme des Merisiers, Saint-Aubin, BP 48, 91192 Gif-sur-Yvette Cédex, France

⁷Madrid Institute of Materials Science (ICMM), CSIC, Cantoblanco, E-28049 Madrid, Spain

and The CSIC Research Associated Unit (MATINEE) between the Institute of Materials Science of the Valencia University (ICMUV)
and the ICMM, 28049 Cantoblanco, Madrid, Spain

⁸Institute of Materials Structure Science, High Energy Accelerator Research Organization (KEK), Tsukuba, Ibaraki 305-0801, Japan

⁹National Institutes for Quantum Science and Technology (QST), Sendai 980-8579, Japan

¹⁰Institute of Multidisciplinary Research for Advanced Materials (IMRAM), Tohoku University, Sendai 980-8577, Japan

¹¹Department of Physics, Kyoto Sangyo University, Kyoto 603-8555, Japan

¹²International Center for Synchrotron Radiation Innovation Smart (SRIS), Tohoku University, Sendai 980-8577, Japan



(Received 13 December 2022; revised 22 March 2023; accepted 24 April 2023; published 6 June 2023)

We have performed micro-/nanofocused angle-resolved photoemission spectroscopy (ARPES) on cleaved single-crystal surfaces of bismuth to clarify the spatially resolved electronic states. While the dominant area of the cleaved surface was found to display the well-known Rashba-spin-split surface state with the (111)-surface origin, the steplike region with a typical width of $\sim 10\text{--}20\ \mu\text{m}$ shows distinctly different band structure and fermiology originating from the hard-to-cleave (100) surface. This unexpected mixture of the (100)-derived electronic states in a tiny area of the cleaved (111) surface is attributed to the crystal planes separated by a twin boundary, as supported by laser microscopy and electron backscatter diffraction measurements. The present study paves a pathway toward investigating electronic states associated with inhomogeneities and coexisting phases of hard-to-cleave crystal planes and complex materials by spatially resolved ARPES, making this technique a powerful method to investigate the interplay between local electronic states and crystal structures when combined with structural characterization techniques.

DOI: [10.1103/PhysRevResearch.5.023152](https://doi.org/10.1103/PhysRevResearch.5.023152)

I. INTRODUCTION

Many quantum phenomena, such as magnetism, superconductivity, and spin/charge density waves, which are central topics in condensed-matter physics, generally appear in homogeneous systems. On the other hand, spontaneously inhomogeneous states (e.g., spatial inhomogeneity, domains, and localized states) have also attracted great deal of attention because they can host exotic quantum phenomena distinct

from the case of homogeneous systems, as highlighted by the quantum Hall effect originating from edge-localized chiral modes [1], two-dimensional (2D) topological-insulator (TI) phases characterized by helical edge modes [2], nanoscale inhomogeneity in cuprates linked to the mechanism of high-temperature superconductivity [3], and electron-hole puddles (inhomogeneity of carrier doping level) in graphene responsible for nonzero minimal electrical conductivity [4]. Besides the investigation of physical properties associated with inhomogeneous states, manipulation of such states, as exemplified by the ferromagnetic-domain-wall motion by electric field [5] and braiding of Majorana bound states in topological superconductors [6], is regarded as a key technology in next-generation electronics and quantum information. It is thus of great importance to explore materials hosting inhomogeneous states.

Group-V element bismuth (Bi), a typical low-carrier semimetal, has a high potential to search for new functionalities originating from the inhomogeneous electronic states. Besides the fundamental interest of bulk Bi in valleytronics

*k.nakayama@arpes.phys.tohoku.ac.jp

†Present address: Shenzhen Institute for Quantum Science and Engineering (SIQSE) and Department of Physics, Southern University of Science and Technology (SUSTech), Shenzhen 518055, China.

‡t-sato@arpes.phys.tohoku.ac.jp

Published by the American Physical Society under the terms of the [Creative Commons Attribution 4.0 International](https://creativecommons.org/licenses/by/4.0/) license. Further distribution of this work must maintain attribution to the author(s) and the published article's title, journal citation, and DOI.

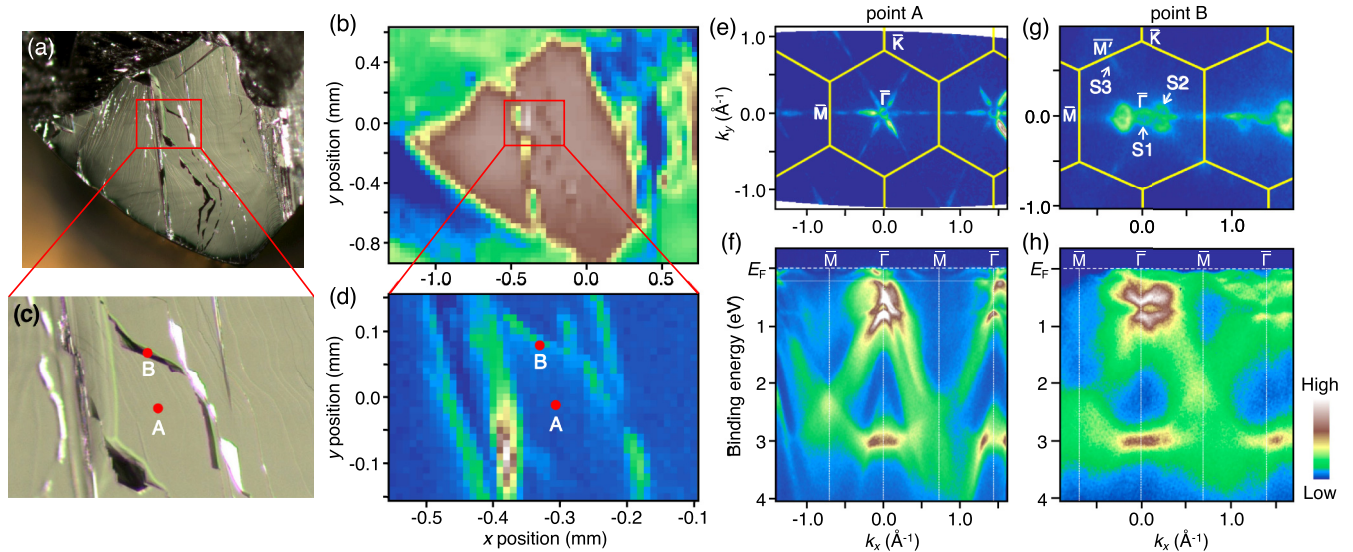


FIG. 1. (a) Photograph of cleaved Bi single-crystal surface, where micro-ARPES measurements were carried out. (b) Corresponding spatial map of ARPES intensity integrated in the (E_B, \mathbf{k}) window of $(E_F \leq E_B \leq 4 \text{ eV}, -1 \text{ \AA}^{-1} \leq k_y \leq 1 \text{ \AA}^{-1} \text{ at } k_x \sim 0)$ measured with $h\nu = 90 \text{ eV}$ at $T = 40 \text{ K}$. (c, d) Same as (a) and (b) but zoomed in the region enclosed by the red rectangle in (a) and (b). To better visualize the steplike feature, color contrast is enhanced in (d). (e, f) Fermi-surface mapping and ARPES intensity obtained along the $\Gamma\bar{M}$ cut of the (111)-surface Brillouin zone, measured at the sample points on the flat surface region [point A in (a) and (c)]. (g, h) Same as (e) and (f), respectively, but measured at a steplike feature [point B in (b) and (d)]. Yellow hexagon in (e) and (g) correspond to the surface Brillouin zones for the (111) and (100) surface, respectively.

[7,8], Bi has attracted particular attention because the crystal surface hosts the spin-split Rashba surface states (SS) associated with the strong spin-orbit coupling (SOC) and breaking of the space-inversion symmetry [9,10] which could be utilized for spintronics application. The strong SOC also makes Bi an indispensable element in many TIs [11–15]. While these properties appear in the spatially homogeneous condition, it has been proposed that Bi hosts exotic inhomogeneous states, such as the edge states in the 2D-TI phase in one to a few bilayers of Bi(111) [16–18], hinge states in higher-order TI phases [19], and twin boundaries formed by the junction of tilted crystal domains [20]. Therefore there is an increasing demand to directly visualize such domains and localized states to establish and understand the exotic properties of Bi.

Besides scanning tunneling microscopy (STM), spatially resolved, angle-resolved photoemission spectroscopy (ARPES) serves as a useful method to access this issue. While conventional ARPES has an insufficient spatial resolution due to the relatively large beam spot size of a few hundred μm , recent remarkable progress in the focusing optics of ARPES end stations in next-generation synchrotron facilities enables us to spatially resolve the electronic states with μm or even sub- μm order [21–26]. Such micro/nano-ARPES has been successfully applied to the measurement of tiny single crystals [27–29], domain-selective observation of layered and 2D materials [30–32], and operando analysis of electronic devices [33,34], and is now becoming a standard tool to investigate spatially resolved electronic states [35]. However, spatially resolved ARPES has not yet been applied to Bi.

In this article we experimentally demonstrate by micro-/nano-ARPES measurements combined with real-space optical microscopy and electron diffraction that a cleaved (111) surface of Bi single crystal contains a twin boundary

with the (100) orientation along the steplike area of the surface. This (100)-derived state cannot be usually obtained by the cleaving and has been completely overlooked in previous ARPES studies. The present study suggests the applicability of spatially resolved ARPES to unveil electronic states of boundary states and hard-to-cleave surface planes, laying a foundation for investigating spatially inhomogeneous states in functional materials.

II. METHODS

Single-crystal Bi was grown by the horizontal melt-growth method with a fused quartz tube. The purity of the raw material shots of Bi is 99.9999% (6N). The melt is placed on a temperature gradient of $\sim 1.5 \text{ K/mm}$ and cooled at a rate of $\sim 0.4 \text{ K/h}$. Spatially resolved ARPES measurements were performed with a Scienta-Omicron DA30 spectrometer at the BL-28A in Photon Factory (PF), KEK and a MBS-A1 electron analyzer at the ANTARES beamline in SOLEIL. We used circularly polarized light of 90 eV and 100 eV in PF and SOLEIL, respectively. Micro-ARPES measurements were performed in PF with a beam spot size of $\phi \sim 10 \mu\text{m}$ achieved by Kirkpatrick-Baez mirror optics [26], whereas nano-ARPES measurements were performed in SOLEIL with a beam spot size of $\phi \sim 400\text{--}500 \text{ nm}$ achieved by a Fresnel-zone-plate focusing system combined with a precise sample scanning system [21]. Bi crystals were cleaved *in situ* along the (111) crystal plane in an ultrahigh vacuum better than $1 \times 10^{-10} \text{ Torr}$. The sample was kept at $T = 40 \text{ K}$ and 60 K in PF and SOLEIL, respectively. Scanning electron microscopy (SEM) and electron back scatter diffraction (EBSD) measurements were performed with a JSM-6610A, JEOL, including a high-resolution slow-scan CCD camera. A

software OIM, EDAX was used for analyzing EBSD patterns. The accelerating voltage of SEM is 20 kV, and the analysis interval of EBSD is 2 μm .

III. RESULTS AND DISCUSSION

We first present the spatial distribution of the electronic structure. Figures 1(a) and 1(b) show an optical microscopy image of the cleaved surface of Bi single crystal and corresponding micro-ARPES intensity map integrated in a wide (E , \mathbf{k}) range, respectively. One can immediately recognize from Fig. 1(a) that while the cleaved surface is dominated by flat regions, several line-shaped, steplike features are also seen, as better visualized by the magnified view in Fig. 1(c). As shown in Fig. 1(b), the ARPES intensity map reflects such steplike features; the flat region seen in the microscope image is characterized by the almost uniform ARPES intensity (light-brown region), whereas the intensity originating from the steplike features appears to be modulated. When we map out the ARPES intensity with finer (x , y) mesh in the area enclosed by red rectangles in Figs. 1(a) and 1(b), one can immediately recognize a good matching between the spatial distribution of steplike features and the ARPES intensity modulation, as shown by a side-by-side comparison of Figs. 1(c) and 1(d). [Note that the contrast of ARPES intensity is enhanced in Fig. 1(d).] This suggests a finite difference in the electronic states between the flat region and the steplike region. When we focus incident photons onto the flat region, the observed electronic structure shows typical characteristics of the (111) surface. This is represented by the Fermi-surface (FS) mapping in Fig. 1(e) and the ARPES intensity along the $\bar{\Gamma}\bar{M}$ cut in Fig. 1(f) measured at representative sample points in the flat region [point A in Figs. 1(c) and 1(d)], where the FS consists of a small circular electron pocket centered at the $\bar{\Gamma}$ point, six elongated hole pockets surrounding the $\bar{\Gamma}$ -centered pocket, and small electron pockets near the \bar{M} point, consistent with the fermiology of Rashba SS reported by previous ARPES studies on bulk crystals and thin films of Bi(111) [9,10,36,37]. On the other hand, when incident photons are focused onto the steplike region [point B in Figs. 1(c) and 1(d)], the FS topology and ARPES intensity are different from those of the flat region, as can be seen from a side-by-side comparison of Figs. 1(e) and 1(g) as well as Figs. 1(f) and 1(h). Specifically, instead of the small pocket at $\bar{\Gamma}$ and surrounding six lobes with the overall sixfold symmetry seen for the (111) surface [Fig. 1(e)], the FS topology for the steplike region [Fig. 1(g)] shows twofold symmetry characterized by a horizontally elongated pocket at the $\bar{\Gamma}$ point, called S1, and vertically elongated small pockets at both sides of this pocket, called S2. Associated with such a clear difference in the FS topology, the band structure for the steplike region [Fig. 1(h)] displays a complicated behavior near E_F , distinct from the relatively simple band structure for the (111) surface [Fig. 1(f)] (see Appendix for details of the band structure near E_F). One may also recognize in Fig. 1(h) a weak intensity away from the S1 and S2 pockets (called S3). We found that the FS topology of all these S1–S3 pockets show a striking agreement with that for the (100) surface obtained by repeating sputter and annealing in the previous work. [Note that the sputter and annealing procedure was used to obtain the (100) surface due

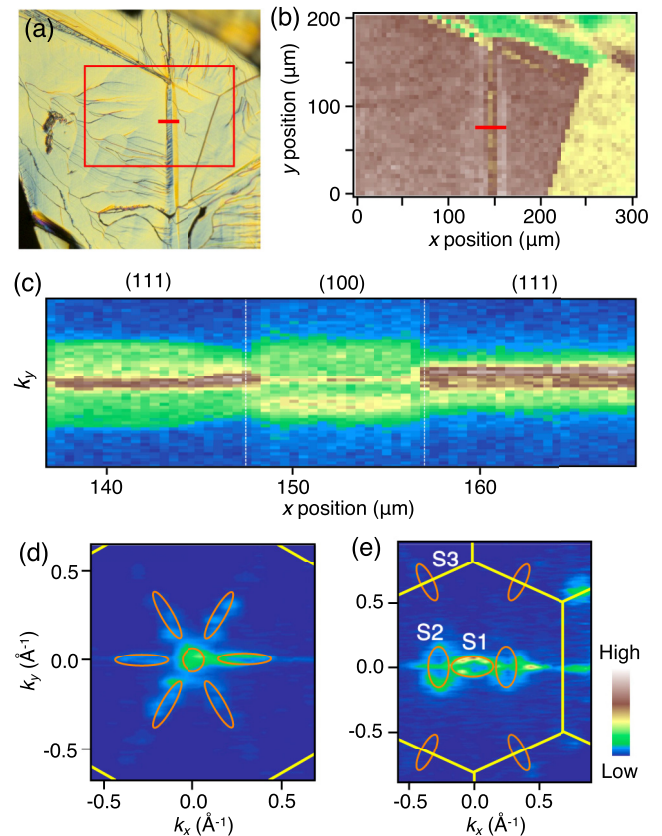


FIG. 2. (a) Optical microscope image of a cleaved Bi single crystal where nano-ARPES measurements were carried out. (b) Spatial map of ARPES intensity integrated in the (E_B , \mathbf{k}) window of ($E_F \leq E_B \leq 4$ eV, $-0.5 \text{ \AA}^{-1} \leq k_y \leq 0.5 \text{ \AA}^{-1}$ at $k_x \sim 0$) in the region enclosed by red rectangle in (a), measured with $h\nu = 100$ eV at $T = 60$ K. (c) ARPES intensity at E_F along the k_y cut plotted against sample position x (y is fixed to $75 \mu\text{m}$) corresponding to red line in (b). (d, e) FS mapping obtained for the (111) and (100) domains, respectively. Open circles and ellipsoids are a guide for the eyes to trace the location of FS.

to the difficulty in cleaving [38].] In fact, when we overlaid the surface Brillouin zone (BZ) of the (100) surface in Fig. 1(g), it shows an excellent matching with the periodicity of the ARPES intensity. In particular, the S1 and S2 pockets seen at $k_x \sim 1.1\text{--}1.6 \text{ \AA}^{-1}$ are nicely on the second BZ of the (100) surface. Also, the S3 pockets are well on the \bar{M} point of the (100) surface BZ. All these results strongly support the (100)-surface origin of the electronic states obtained in the steplike region.

To clarify whether or not such unexpected mixture of the (100) states is reproducible for different cleaves and different samples, we have performed another ARPES experiment using a nano-ARPES system with a Bi single crystal obtained from a different sample batch. One can again recognize from an optical microscope image for the cleaved surface in Fig. 2(a) that two prominent steplike features run vertically and along another direction 120° rotated from it. The ARPES intensity map in Fig. 2(b) obtained in the region enclosed by the red square in Fig. 2(a) shows a good correspondence with the microscope image; in particular, the intensity of the

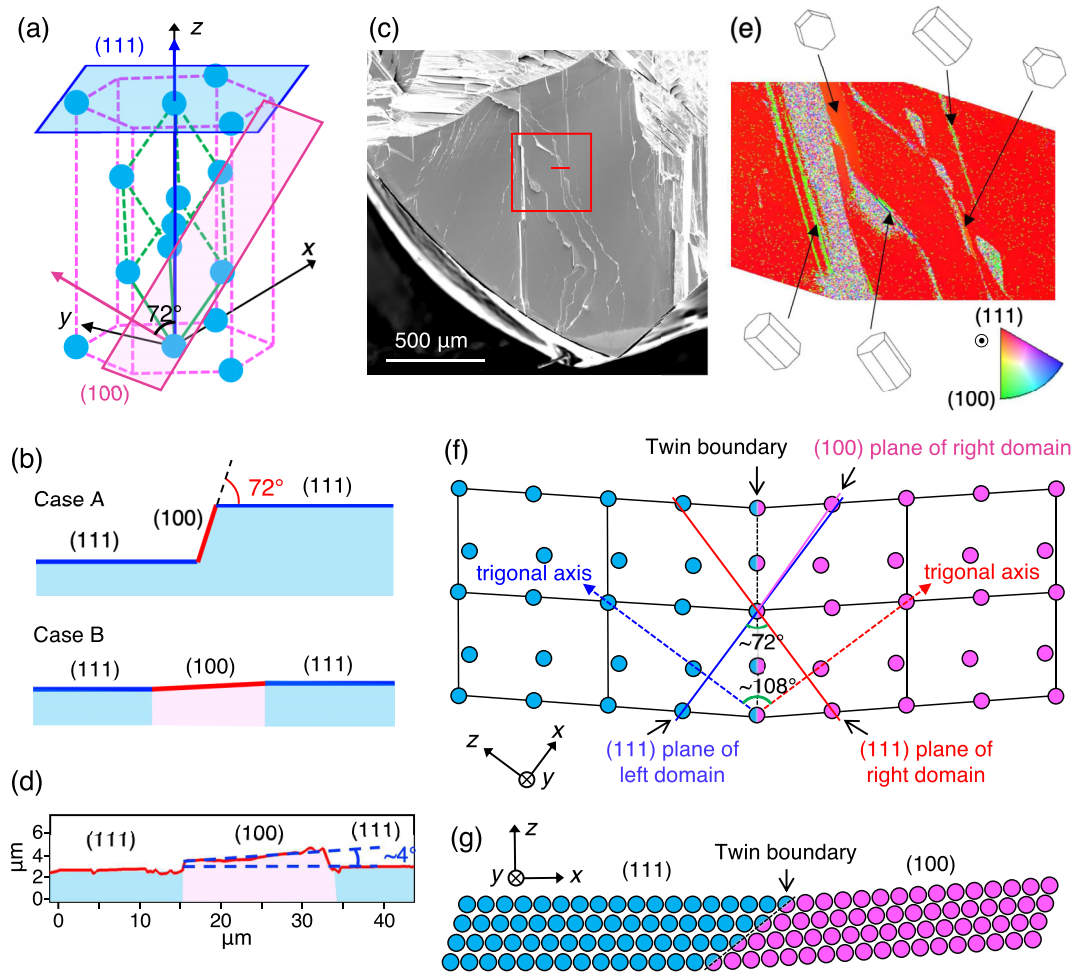


FIG. 3. (a) Schematic crystal structure of Bi, together with the (111) and (100) crystal planes (rectangles). The blue and magenta arrows correspond to the direction normal to the (111) and (100) planes, respectively. (b) Two possible cases of (100) domains faced to two (111) domains. In the top panel, the crystal globally maintains the single-phased crystallinity, so that the angle (θ) between (111) and (100) planes is 72° . In the bottom panel, the crystal contains two phases with different orientations, so that θ does not necessarily keep 72° . (c) Scanning electron microscopy image of cleaved crystal where micro-APRES was carried out. (d) Height profile measured along a spatial cut crossing the boundaries of (111) and (100) domains [red line in (c)] obtained by laser microscope. (e) SEM-EBSD image obtained in the area enclosed by a red box in (c). Color indicates crystal orientation of normal direction. (f) Schematic of twin structure in Bi [40]. (g) Schematic of atomic arrangement at the surface across the twin boundary of Bi.

steplike region is modulated with respect to the surrounding flat surface region, consistent with the micro-ARPES data shown in Fig. 1(b). As shown in Fig. 2(c), the ARPES intensity at E_F along the k_y cut, measured along the sample positions crossing this steplike feature [indicated by the red line in Figs. 2(a) and 2(b)] signifies discontinuous transitions of the intensity profile at the boundaries of the steplike feature and flat region. From the observed difference in the symmetry of the FS image (C_6 vs C_2) shown in Figs. 2(d) and 2(e), the flat and steplike regions are assigned to the (111) and (100) surfaces, respectively, consistent with the micro-ARPES data shown in Fig. 1. These indicate the reproducibility of our ARPES results. It is noted that we measured four millimeter-sized samples, including those displayed in Figs. 1 and 2, and observed the (100) domain in all of them. This implies that the (100) domain always appears on the surface when the cleaved crystal surface is much larger than the (100) domain size

(typically, several hundred μm in our samples). The fraction of the (100) domain is 11% and 8% in Figs. 1(d) and 2(b), respectively. Since these data were obtained at the position where the (100) domain is prominent, the mean fraction of the (100) domain over the entire sample surface is expected to be lower.

Now that the inclusion of (100)-derived electronic states in the cleaved (111) surface is experimentally established, next we discuss the origin of this state. As shown by the crystal structure of Bi in Fig. 3(a), the (111) and (100) planes are rotated by 72° from each other. Thus, one explanation is that this tilted (100) plane is locally obtained by accidental cleaving, despite its hard-to-cleave nature. In this case, since the crystal fully keeps the single orientation, the tiny (100) region is exposed with the tilt angle of 72° with respect to the (111) region, as schematically shown in the top panel of Fig. 3(b) (called case A). On the other hand, if the (100) region has a

different orientation than the rest due to the local inclusion of different crystal domains in the sample, the tilt angle between the (100) and (111) regions is not necessarily restricted to 72° [bottom panel of Fig. 3(b); case B]. To clarify the correct model, we have carried out laser microscopy measurements and obtained a height profile along a cut crossing the steplike feature [red line shown by SEM image in Fig. 3(c)]. The result shown in Fig. 3(d) signifies that the (100) plane has a width of $\sim 20 \mu\text{m}$ and has a tilt angle of $\sim 4 \pm 3^\circ$, far from 72° . [Note that the small tilt angle was also confirmed by ARPES by comparing the sample rotation angle at the Γ point between the (111) and (100) surfaces.] This suggests that case B is actually realized.

To further validate above conclusion, we have performed SEM-EBSD measurements on the sample area where the ARPES spatial mapping was performed. Figure 3(e) shows the obtained result in which different crystal orientations are shown by different colorings. One can see that the surface region is dominated by the (111) plane shown by the red color, as expected from the ARPES data in Fig. 1. On the other hand, there exist several lines with the green color. Intriguingly, the spatial location of such lines shows a good agreement with the steplike feature seen as a modulation of intensity in the spatial mapping of ARPES intensity in Fig. 1(d), supporting the non-(111) origin of the steplike feature. We found from the analysis of SEM-EBSD data that such an area mostly originates from the (100) plane, consistent with the ARPES result.

The rhombohedral structure of Bi [Fig. 3(a)] can be viewed as a distorted cubic lattice which is obtained by pulling a simple cubic crystal along one of the four trigonal axes, leaving only one trigonal axis [defined as the z axis in Fig. 3(a)]. Depending on the direction of lattice distortion, maximally four (111) crystal domains can exist, and when more than two domains are included in the crystal, a twin boundary will be formed at their intersection [39,40]. It was reported that the tilt angle between the trigonal axes of the adjacent domains across the twin boundary is $\sim 108^\circ$ [39,40], as schematically shown in Fig. 3(f), where the trigonal axes of the left and right domains are indicated by dashed blue and red arrows, respectively. Therefore the angle between the (111) planes of the left and right domains [solid blue and red lines, respectively, in Fig. 3(f)] is $\sim 72^\circ$, indicating a near coincidence of the (111) plane of the left domain to the (100) plane of the right domain [see solid blue and magenta lines in Fig. 3(f), the latter of which corresponds to the (100) plane of the right domain; note that the (111) plane of the right domain almost coincides with the (100) plane of the left domain (not shown)]. Consequently, when the crystal is cleaved along the (111) plane of the left domain [parallel to the solid blue line in Fig. 3(f)], the (100) surface of the right domain can be exposed with almost negligible surface tilting [possibly a vicinal (100) surface consisting of large (100) terraces and small steps with different orientations], in good agreement with the ARPES results and structural analysis. [See schematic for the cleaved surface across the twin boundary in Fig. 3(g), in which the crystal orientation is rotated from that in Fig. 3(f), so the horizontal direction in Fig. 3(g) (x axis) is parallel to the solid blue line in Fig. 3(f).] It is thus concluded that the (100)-derived electronic states seen by micro-/nano-ARPES originate from the crystal twin boundary. [Note that although the twinning of

Bi crystals was reported, no previous works clearly indicated that the twin-originated domain appears on the surface as the (100) plane, and it was also unclear whether well-defined surface states are formed there.] The present study thus clarifies the band structure of the crystal twin boundary in Bi. The existence of twin domains with distinct electronic states would support the proposal to explain the unusual Landau spectrum [20]. It is also emphasized here that since the twin boundary has the (100) [or a vicinal (100)] orientation which is hardly obtained by the cleaving, investigation of such a state provides a precious opportunity to study the characteristics of crystal planes hard to be accessed by conventional methods.

In the above discussion [Figs. 3(f) and 3(g)], we assumed that the crystal plane which is nearly parallel to the (111) plane of the left domain is preferentially exposed in the right domain. Other hard-to-cleave surfaces (especially, low-index surfaces) have relatively large angle mismatch with the (111) plane of the left domain, e.g., $\sim 52^\circ$ for the (110) plane, and hence would rarely appear near the twin boundary. Nevertheless, the surface orientation in the right domain may eventually change [probably to the (111) plane] on going away from the twin boundary because the (100) plane is not the natural cleaving plane. Such a change would limit the width of the (100) domains (their smaller volume fraction in the crystal is another factor to limit the domain size).

Based on the present results, it is strongly suggested that spatially resolved ARPES serves as a useful method to visualize spatially inhomogeneous electronic states. When combined with the crystal structure characterization such as SEM-EBSD, it becomes even more powerful to study the interplay between the electronic and crystal structures. While we demonstrated the applicability of this technique by visualizing the twin boundary, it could be useful to unveil other local modulations of electronic and crystal structures, such as dislocations, stacking faults, dielectric domains, and edge- or hinge-localized states, when sufficient spatial resolution is

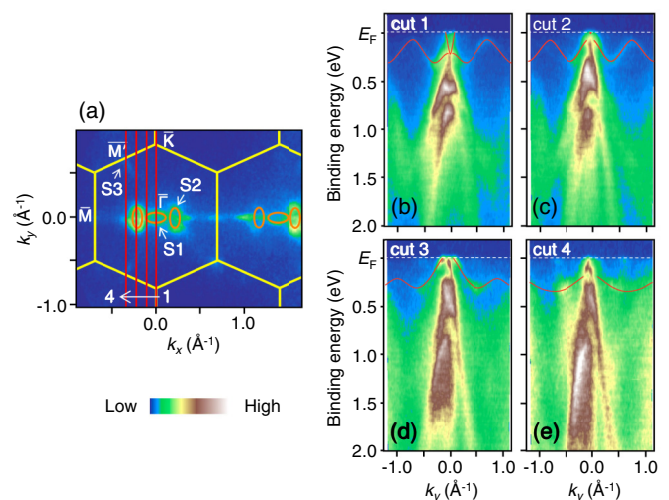


FIG. 4. (a) Fermi-surface mapping obtained in a steplike region on the cleaved surface of Bi [same as Fig. 1(g) in the main text]. [(b),(e)] Intensity plots as a function of wave vector and binding energy measured along four representative k cuts shown by red lines in (a).

obtained. It is thus strongly desirable to apply this technique to a wide variety of materials to explore new functionalities associated with the spatially inhomogeneous electronic states.

IV. CONCLUSIONS

In conclusion, the present micro/nano-ARPES study has revealed unexpected local inclusion of the (100)-derived electronic states for the Bi(111) surface. By combining laser microscopy and SEM-EBSD measurements, we found that this state originates from the crystal twin boundary. The present study opens a pathway toward investigating the interplay between local electronic and crystal structures by directly visualizing local modulation of electronic states hard to be accessed by conventional techniques.

ACKNOWLEDGMENTS

This work was supported by JST-CREST (No. JPMJCR18T1), JST-PRESTO (No. JPMJPR18L7),

JSPS KAKENHI Grants No. JP21H04435, No. JP21K03434, and No. JP20H01847, KEK-PF (Proposal No. 2021S2-001), SOLEIL (Proposal No. 20190458), and World Premier International Research Center, Advanced Institute for Materials Research. T.K. acknowledges support from GP-Spin at Tohoku University and a JSPS fellowship (No. JP22KJ0270).

APPENDIX: BAND STRUCTURE IN THE STEPLIKE REGION

The Fermi surface measured in the steplike region of the cleaved Bi surface [Fig. 4(a)] shows a horizontally elongated pocket at the $\bar{\Gamma}$ point (S1) and vertically elongated small pockets at both sides of this pocket (S2). Figures 4(b)–4(e) show the intensity plots obtained along k cuts 1–4 in Fig. 4(a), respectively. From the k cuts crossing the S1 and S2 pockets [cuts 1 and 3 in Fig. 4(a)], the S1 and S2 bands are assigned to the electron and hole pockets, respectively.

-
- [1] K. V. Klitzing, G. Dorda, and M. Pepper, New Method for High-Accuracy Determination of the Fine-Structure Constant Based on Quantized Hall Resistance, *Phys. Rev. Lett.* **45**, 494 (1980).
- [2] M. König, S. Wiedmann, C. Brüne, A. Roth, H. Buhmann, L. W. Molenkamp, X.-L. Qi, and S.-C. Zhang, Quantum spin Hall insulator state in HgTe quantum wells, *Science* **318**, 766 (2007).
- [3] K. M. Lang, V. Madhavan, J. E. Hoffman, E. W. Hudson, H. Eisaki, S. Uchida, and J. C. Davis, Imaging the granular structure of high- T_c superconductivity in underdoped $\text{Bi}_2\text{Sr}_2\text{CaCu}_2\text{O}_{8+\delta}$, *Nature (London)* **415**, 412 (2002).
- [4] J. Martin, N. Akerman, G. Ulbricht, T. Lohmann, J. H. Smet, K. V. Klitzing, and A. Yacoby, Observation of electron-hole puddles in graphene using a scanning single-electron transistor, *Nat. Phys.* **4**, 144 (2008).
- [5] D. A. Allwood, G. Xiong, C. C. Faulkner, D. Atkinson, D. Petit, and R. P. Cowburn, Magnetic domain-wall logic, *Science* **309**, 1688 (2005).
- [6] A. Y. Kitaev, Fault-tolerant quantum computation by anyons, *Ann. Phys.* **303**, 2 (2003).
- [7] Z. Zhu, A. Collaudin, B. Fauqué, W. Kang, and K. Behnia, Field-induced polarization of Dirac valleys in bismuth, *Nat. Phys.* **8**, 89 (2012).
- [8] R. Küchler, L. Steinke, R. Daou, M. Brando, K. Behnia, and F. Steglich, Thermodynamic evidence for valley-dependent density of states in bulk bismuth, *Nat. Mater.* **13**, 461 (2014).
- [9] Y. M. Koroteev, G. Bihlmayer, J. E. Gayone, E. V. Chulkov, S. Blügel, P. M. Echenique, and Ph. Hofmann, Strong Spin-Orbit Splitting on Bi Surfaces, *Phys. Rev. Lett.* **93**, 046403 (2004).
- [10] Ph. Hofmann, The surfaces of bismuth: Structural and electronic properties, *Prog. Surf. Sci.* **81**, 191 (2006).
- [11] L. Fu and C. L. Kane, Topological insulators with inversion symmetry, *Phys. Rev. B* **76**, 045302 (2007).
- [12] H. Zhang, C.-X. Liu, X.-L. Qi, X. Dai, Z. Fang, and S.-C. Zhang, Topological insulators in Bi_2Se_3 , Bi_2Te_3 and Sb_2Te_3 with a single Dirac cone on the surface, *Nat. Phys.* **5**, 438 (2009).
- [13] M. Z. Hasan and C. L. Kane, Colloquium: Topological insulators, *Rev. Mod. Phys.* **82**, 3045 (2010).
- [14] X.-L. Qi and S.-C. Zhang, Topological insulators and superconductors, *Rev. Mod. Phys.* **83**, 1057 (2011).
- [15] Y. Ando, Topological insulator materials, *J. Phys. Soc. Jpn.* **82**, 102001 (2013).
- [16] S. Murakami, Quantum Spin Hall Effect and Enhanced Magnetic Response by Spin-Orbit Coupling, *Phys. Rev. Lett.* **97**, 236805 (2006).
- [17] Z. Liu, C.-X. Liu, Y.-S. Wu, W.-H. Duan, F. Liu, and J. Wu, Stable Nontrivial Z_2 Topology in Ultrathin Bi (111) Films: A First-Principles Study, *Phys. Rev. Lett.* **107**, 136805 (2011).
- [18] I. K. Drozdov, A. Alexandradinata, S. Jeon, S. Nadj-Perge, H. Ji, R. J. Cava, B. A. Bernevig, and A. Yazdani, One-dimensional topological edge states of bismuth bilayers, *Nat. Phys.* **10**, 664 (2014).
- [19] F. Schindler, Z. Wang, M. G. Vergniory, A. M. Cook, A. Murani, S. Sengupta, A. Y. Kasumov, R. Deblock, S. Jeon, I. Drozdov, H. Bouchiat, S. Guéron, A. Yazdani, B. A. Bernevig, and T. Neupert, Higher-order topology in bismuth, *Nat. Phys.* **14**, 918 (2018).
- [20] Z. Zhu, B. Fauqué, L. Malone, A. B. Antunes, Y. Fuseya, and K. Behnia, Landau spectrum and twin boundaries of bismuth in the extreme quantum limit, *Proc. Natl. Acad. Sci. USA* **109**, 14813 (2012).
- [21] J. Avila, A. Boury, B. Caja-Muñoz, C. Chen, S. Lorcy, and M. C. Asensio, Optimal focusing system of the Fresnel zone plates at the Synchrotron SOLEIL NanoARPES Beamline, *J. Phys.: Conf. Ser.* **849**, 012039 (2017).
- [22] R. J. Koch, C. Jozwiak, A. Bostwick, B. Stripe, M. Cordier, Z. Hussain, W. Yun, and E. Rotenberg, Nano focusing of soft X-rays by a new capillary mirror optic, *Synchrotron Radiat. News* **31**, 50 (2018).
- [23] H. Iwasawa, P. Dudin, K. Inui, T. Masui, T. K. Kim, C. Cacho, and M. Hoesch, Buried double CuO chains in $\text{YBa}_2\text{Cu}_4\text{O}_8$ uncovered by nano-ARPES, *Phys. Rev. B* **99**, 140510(R) (2019).

- [24] P. Dudin, P. Lacovig, C. Fava, E. Nicolini, A. Bianco, G. Cautero, and A. Barinov, Angle-resolved photoemission spectroscopy and imaging with a submicrometre probe at the SPECTROMICROSCOPY-3.2L beamline of Elettra, *J. Synchrotron Radiat.* **17**, 445 (2010).
- [25] M. Hoesch, T. K. Kim, P. Dudin, H. Wang, S. Scott, P. Harris, S. Patel, M. Matthews, D. Hawkins, S. G. Alcock, T. Richter, J. J. Mudd, M. Basham, L. Pratt, P. Leicester, E. C. Longhi, A. Tamai, and F. Baumberger, A facility for the analysis of the electronic structures of solids and their surfaces by synchrotron radiation photoelectron spectroscopy, *Rev. Sci. Instrum.* **88**, 013106 (2017).
- [26] M. Kitamura, S. Souma, A. Honma, D. Wakabayashi, H. Tanaka, A. Toyoshima, K. Amemiya, T. Kawakami, K. Sugawara, K. Nakayama, K. Yoshimatsu, H. Kumigashira, T. Sato, and K. Horiba, Development of a versatile micro-focused angle-resolved photoemission spectroscopy system with Kirkpatrick-Baez mirror optics, *Rev. Sci. Instrum.* **93**, 033906 (2022).
- [27] J. Avila, I. Razado, S. Lorcy, R. Fleurier, E. Pichonat, D. Vignaud, X. Wallart, and M. A. Asensio, Exploring electronic structure of one-atom thick polycrystalline graphene films: A nano angle resolved photoemission study, *Sci. Rep.* **3**, 2439 (2013).
- [28] J. Krieg, C. Chen, J. Avila, Z. Zhang, W. Sigle, H. Zhang, C. Trautmann, M. C. Asensio, and M. E. Toimil-Molares, Exploring the electronic structure and chemical homogeneity of individual Bi_2Te_3 nanowires by nano-angle-resolved photoemission spectroscopy, *Nano Lett.* **16**, 4001 (2016).
- [29] D. Takane, Z. Wang, S. Souma, K. Nakayama, T. Nakamura, H. Oinuma, Y. Nakata, H. Iwasawa, C. Cacho, T. Kim, K. Horiba, H. Kumigashira, T. Takahashi, Y. Ando, and T. Sato, Observation of Chiral Fermions with a Large Topological Charge and Associated Fermi-Arc Surface States in CoSi , *Phys. Rev. Lett.* **122**, 076402 (2019).
- [30] C. Chen, J. Avila, S. Wang, Y. Wang, M. Mucha-Kruczyński, X. Shen, R. Yang, B. Nosarzewski, T. P. Devereaux, G. Zhang, and M. C. Asensio, Emergence of interfacial polarons from electron-phonon coupling in graphene/h-BN van der Waals heterostructures, *Nano Lett.* **18**, 1082 (2018).
- [31] K. Nakayama, S. Souma, C. X. Trang, D. Takane, C. Chen, J. Avila, T. Takahashi, S. Sasaki, K. Segawa, M. C. Asensio, Y. Ando, and T. Sato, Nanomosaic of topological Dirac states on the surface of $\text{Pb}_5\text{Bi}_{24}\text{Se}_{41}$ observed by nano-ARPES, *Nano Lett.* **19**, 3737 (2019).
- [32] R. Noguchi, T. Takahashi, K. Kuroda, M. Ochi, T. Shirasawa, M. Sakano, C. Bareille, M. Nakayama, M. D. Watson, K. Yaji, A. Harasawa, H. Iwasawa, P. Dudin, T. K. Kim, M. Hoesch, V. Kandyba, A. Giampietri, A. Barinov, S. Shin, R. Arita *et al.*, A weak topological insulator state in quasi-one-dimensional bismuth iodide, *Nature (London)* **566**, 518 (2019).
- [33] P. V. Nguyen, N. C. Teutsch, N. P. Wilson, J. Kahn, X. Xia, A. J. Graham, V. Kandyba, A. Giampietri, A. Barinov, G. C. Constantinescu, N. Yeung, N. D. M. Hine, X. Xu, D. H. Cobden, and N. R. Wilson, Visualizing electrostatic gating effects in two-dimensional heterostructures, *Nature (London)* **572**, 220 (2019).
- [34] F. Joucken, J. Avila, Z. Ge, E. A. Quezada-Lopez, H. Yi, R. L. Goff, E. Baudin, J. L. Davenport, K. Watanabe, T. Taniguchi, M. C. Asensio, and J. Velasco, Jr., Visualizing the effect of an electrostatic gate with angle-resolved photoemission spectroscopy, *Nano Lett.* **19**, 2682 (2019).
- [35] H. Zhang, T. Pincelli, C. Jozwiak, T. Kondo, R. Ernstorfer, T. Sato, and S. Zhou, Angle-resolved photoemission spectroscopy, *Nat. Rev. Meth. Primers* **2**, 54 (2022).
- [36] T. Hirahara, T. Nagao, I. Matsuda, G. Bihlmayer, E. V. Chulkov, Y. M. Koroteev, P. M. Echenique, M. Saito, and S. Hasegawa, Role of Spin-Orbit Coupling and Hybridization Effects in the Electronic Structure of Ultrathin Bi Films, *Phys. Rev. Lett.* **97**, 146803 (2006).
- [37] A. Takayama, T. Sato, S. Souma, and T. Takahashi, Giant Out-of-Plane Spin Component and the Asymmetry of Spin Polarization in Surface Rashba States of Bismuth Thin Film, *Phys. Rev. Lett.* **106**, 166401 (2011).
- [38] Ph. Hofmann, J. E. Gayone, G. Bihlmayer, Yu. M. Koroteev, and E. V. Chulkov, Electronic structure and Fermi surface of $\text{Bi}(100)$, *Phys. Rev. B* **71**, 195413 (2005).
- [39] E. O. Hall, *Twinning and Diffusionless Transformations in Metals* (Butterworth Scientific Publishing, London, 1954), cited in M. V. Klassen-Neklyudova, *Mekhanicheskoe Dvoynikovanie Kristallov (Mechanical Twinning of Crystals)* (Akad. Nauk SSSR, Moscow, 1960).
- [40] V. S. Edelman, D. Y. Sharvin, I. N. Khlyustikov, and A. M. Troyanovskii, STM revealing of twin microlayers with quantized width on cleaved bismuth surface, *Europhys. Lett.* **34**, 115 (1996).